ChemComm

COMMUNICATION

View Article Online
View Journal | View Issue

Cite this: *Chem. Commun.*, 2019, **55**, 636

Received 20th November 2018,
Accepted 8th December 2018

DOI: 10.1039/c8cc09207a

rsc.li/chemcomm

Sequence isomeric giant surfactants with distinct self-assembly behaviors in solution†

Wei Zhang,[a] Wenpeng Shan,[a] Shuailin Zhang,[a] Yuchu Liu,[a] Hao Su,[b] Jiancheng Luo,[a] Yanfeng Xia,[a] Tao Li,[cd] Chrys Wesdemiotis,[ae] Tianbo Liu,[a] Honggang Cui,[b] Yiwen Li*[f] and Stephen Z. D. Cheng*[ag]

We have designed and synthesized a pair of sequence isomeric giant surfactants based on polystyrene (PS) and polyhedral oligomeric silsesquioxane (POSS) nanoparticles. Although these two macromolecules possess identical compositions as "sequence isomers", the distinctly arranged POSS sequences lead to different molecular packing conformations, and further induce distinguished self-assembly behaviors in DMF/water solutions.

Design and synthesis of sequence-defined macromolecules has attracted a lot of attention in recent years and still remains very challenging. In the synthetic aspect, quite a few elegant approaches have been developed.[1–9] For instance, Meier *et al.* developed a method to synthesize sequence-controlled oligomers through the Passerini three-component reaction.[10] Lutz and co-workers synthesized sequence-coded polymers with molecular masses >10kDa based on the phosphoramidite coupling reaction.[11,12] Zhang's group achieved sequence-controlled polymers using furan-protected maleimide as a latent monomer.[13] Although the sequence has been well known to be one of the key molecular parameters to determine the structures and properties in biomacromolecules, such as peptides, peptoids and nucleic acids,[14–18] there are only a limited number of works regarding the sequence effect on synthetic macromolecules.[19–22] Johnson *et al.* very recently demonstrated that the stereochemical sequence could dictate unimolecular diblock copolymer assembly in the bulk.[23] Our group has developed sequence-controlled "giant molecules", which are precisely defined macromolecules in terms of stereochemistry, composition, sequence, topology and molecular mass built on molecular nanoparticles (MNP) such as polyhedral oligomeric silsesquioxane (POSS) nanoparticles.[24–26] Using POSS nanoparticles as macromonomers, the sequence effect of giant molecules can be amplified, and versatile distinct phase structures, including unconventional Frank–Kasper A15, sigma and dodecagonal quasicrystal structures, have been obtained from the sequence isomers in the solid state.[24,27] It could also be interesting to investigate the sequence effect of synthetic macromolecules on their self-assembly behaviors in solution or thin film states.

In another aspect, the solution self-assembly behaviors of giant surfactants have been widely investigated by our group.[28–30] Giant surfactants are a class of precisely defined amphiphilic macromolecules composed of MNP heads and polymer tails. These giant surfactants capture the essential feature of small molecular surfactants while possessing much larger sizes.[28] They are thus bridging the gap between traditional amphiphilic block copolymers and small molecular surfactants. Several macromolecular parameters, such as the molecular composition and topology, have been demonstrated to play important roles in the self-assembly behaviors of giant surfactants in solution.[30–33] To further advance our understanding, how the sequence, as another molecular parameter, affects the solution assembly of giant surfactants remains to be explored. In this letter, we have prepared a pair of polystyrene (PS) and POSS-based "sequence isomers" PS-$(BPOSS)_2$(APOSS) and PS-(APOSS)$(BPOSS)_2$ (denoted PS-BBA and PS-ABB, where B represents BPOSS with seven isobutyl groups at the corners of the POSS core, and A represents APOSS with seven carboxylic acid groups at the corners of the POSS core) to explore the effect of the sequence in giant surfactants.

The polymer–POSS conjugates are synthesized through iteratively performed strain-promoted alkyne cycloadditions (SPACC) and oxime ligations as previously reported.[8] Their molecular structures

[a] *Department of Polymer Science, College of Polymer Science and Polymer Engineering, The University of Akron, Akron, Ohio, 44325-3909, USA. E-mail: scheng@uakron.edu*
[b] *Department of Chemical and Biomolecular Engineering, The Johns Hopkins University, Baltimore, MD 21218, USA*
[c] *Department of Chemistry and Biochemistry, Northern Illinois University, DeKalb, IL 60115, USA*
[d] *X-ray Science Division, Advanced Photon Source, Argonne National Laboratory, Argonne, Illinois, 60439, USA*
[e] *Department of Chemistry, The University of Akron, Akron, Ohio 44325-3601, USA*
[f] *College of Polymer Science and Engineering, State Key Laboratory of Polymer Materials Engineering, Sichuan University, Chengdu, 610065, China. E-mail: ywli@scu.edu.cn*
[g] *South China Advanced Institute for Soft Matter Science and Technology, South China University of Technology, Guangzhou, 510640, China*

† Electronic supplementary information (ESI) available. See DOI: 10.1039/c8cc09207a

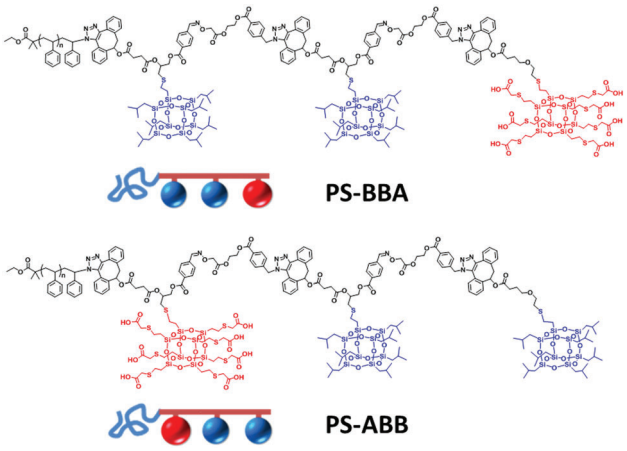

Fig. 1 Molecular structures of PS-ABB and PS-BBA.

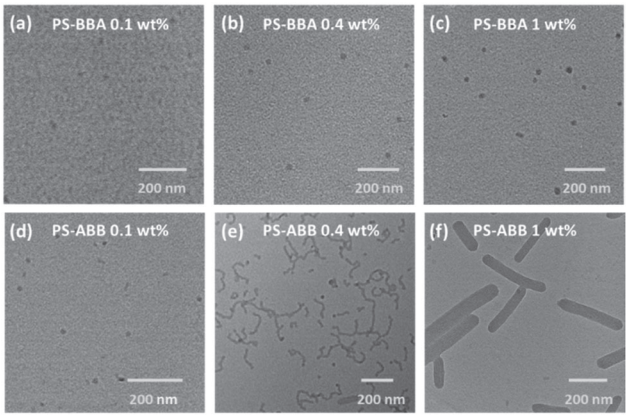

Fig. 2 TEM images of the assembled structures of PS-BBA (a–c) and PS-ABB (d–f) at initial concentrations of 0.1 wt%, 0.4 wt% and 1 wt%, respectively.

are shown in Fig. 1. The detailed synthetic route is provided in the ESI.† The building blocks such as DIBO-B-CHO, DIBO-V-CHO, DIBO-B, and DIBO-V and the "click adaptor" were prepared as previously described.[8,27] An azido terminated polystyrene (PS-N_3) with a molecular weight of 2k is used as the starting material. Then, two BPOSSs are installed onto the polymer chain-end through two reaction cycles of SPAAC and oxime ligations, followed by attaching one more VPOSS, which has seven vinyl groups at each corner and is the precursor of APOSS. As the POSS NPs are attached onto the polymer chains, in the ^{1}H NMR spectra, the characteristic signals from BPOSS (δ 1.8–1.9 ppm for –C*H*(CH_3)$_2$) and VPOSS (δ 5.8–6.2 ppm for –C*H*=C*H*$_2$) appear clearly as shown in Fig. S1a (ESI†), and the GPC curves exhibit clear shift toward low retention times, indicating an increase of molecular weight (Fig. S1b, ESI†). Furthermore, a matrix-assisted laser desorption ionization time-of-flight (MALDI-TOF) mass spectrum also shows consistent molecular weight compared to the calculated molecular weight with a single distribution with a distance of 104 Da, which corresponds to a styrene repeat unit (Fig. S1c, ESI†). Finally, VPOSS is converted into APOSS *via* thiol–ene click reaction[34] to afford PS-BBA (Scheme S2, ESI†). Its "sequence isomer" PS-ABB can be synthesized in a similar way but just with the incorporation of VPOSS or BPOSS in a different step (Scheme S3, ESI†). Due to the same chemical composition, these two macromolecules show almost identical NMR, GPC and MALDI-TOF spectra (Fig. S2–S5, ESI†).

In the solution assembly study, dimethylformamide (DMF) was used as the common solvent for both the hydrophilic and hydrophobic parts to dissolve the materials at different initial concentrations, then water was added very slowly into the system as we previously described for PS-(APOSS)$_n$ samples.[29,31] In order to directly compare the influences of the sequence on these two giant molecules, we used exactly identical conditions to prepare micellar samples, including initial concentrations of 0.1 wt%, 0.4 wt% and 1 wt%, respectively. It was observed in the transmission electron microscopy (TEM) results that PS-BBA can only form spherical aggregates at different initial concentrations in the experiments (Fig. 2a–c). However, it is very interesting to note that its "sequence isomer" PS-ABB shows different assembly morphologies. For example, at a low concentration (0.1 wt%), it also forms spherical assemblies (Fig. 2d). As the initial concentration increases to 0.4 wt%, it forms cylindrical assemblies (Fig. 2e). Upon further increasing the initial concentration to 1 wt%, it could form ribbon-like assemblies instead of traditional vesicular structures as shown in Fig. 2f.

By looking at the ribbon-like assemblies in detail, phase separated lamellar structures exist with a spacing of about 10 nm. The ribbon-like structure is further confirmed by cryo-TEM to exclude the drying effects (Fig. 3a). The lengths of the ribbon-like assemblies are several hundreds of nanometers with widths around 70–100 nm from the TEM results. The thickness of the ribbon-like assemblies is measured to be about 25 nm using atomic force microscopy (AFM) (Fig. 3b and c).

The concept of the packing parameter (p) established in the self-assembly of small molecular surfactant systems can also be applied to evaluate giant surfactants.[29–31] It is defined as $p = V/(a \times l)$, where V, l and a are the volume and length of the hydrophobic tail, and the cross-sectional area of the hydrophilic head group, respectively.[35] Three regions of the p values ($p < 0.33$, $0.33 < p < 0.5$, and $p > 0.5$) usually indicate spherical micelles,

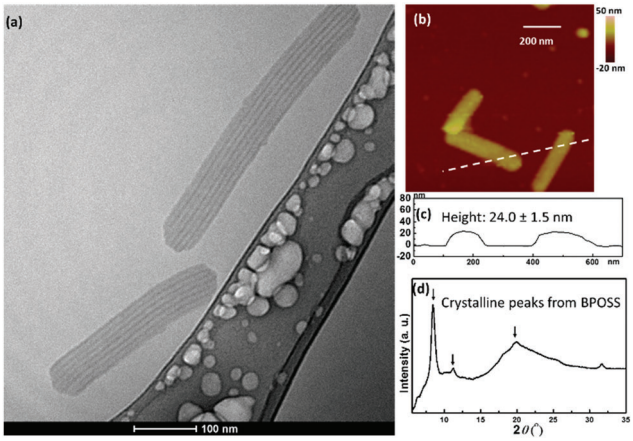

Fig. 3 Characterization of the ribbon-like structure of PS-ABB: (a) cryo-TEM image; (b) AFM image; (c) height profile and (d) wide angle X-ray diffraction.

cylindrical micelles and vesicles/lamellae, respectively. Our previous work has demonstrated that the initial concentration of giant surfactants is one of the parameters determining the final assembled structure *via* the degree of ionization of carboxylic acid groups on APOSS, which decreases as the initial concentration increases.[30] This results in the reduction of the effective head size and cross-sectional area of the surfactant, finally leading to an increase of p.[31]

For these two sequence isomeric giant surfactants, the volumes of the hydrophobic parts (V) are identical and can be estimated to be 5.6 nm^3 by the following calculation:

$$V = V_B + V_{PS} = \frac{M_B}{N_A \rho_B} + \frac{M_{PS}}{N_A \rho_{PS}},$$

where V_B and V_{PS} are the volumes of the BPOSS and PS parts, respectively; M_B = 1.6 kg mol^{-1} (for simplification we include the linker as well) and M_{PS} = 2 kg mol^{-1} are the molecular masses of the BPOSS and PS parts, respectively; ρ_B = 1.1 g cm^{-3} and ρ_{PS} = 1.04 g cm^{-3} are their densities;[36] and N_A is the Avogadro constant.

Polymer tails in giant surfactants have been previously found to be highly stretched especially for low molecular weights, which is different from most traditional amphiphilic block copolymers.[29] So, for simplified qualitative analysis of the difference in self-assembly behavior, the contour length of the polystyrene tail (l_{PS}) in this work can be estimated to be about 5 nm by l = 0.154n sin(109.5°/2), where n = 40 (two carbons per repeat unit). The length of the BPOSS part with the linkers (l_B) is also about 5 nm. When we assume no ionization condition, the smallest cross-sectional area of APOSS (a_A) can be estimated to be 1.8 nm^2 based on its diameter of about 1.5 nm. In the self-assembly of PS-BBA, the hydrophobic BPOSS and PS are on the same side of APOSS, and thus, they could stay together in the hydrophobic core. This molecule resembles a "one-head one-tail" giant surfactant. As the initial concentration increases, the degree of ionization of carboxylic acids on APOSS decreases, which leads to a decrease of effective head size and a_A,[31] so that p becomes larger. Note that p reaches the maximum possible value by assuming no ionization of APOSS and the polar head becomes the smallest volume. It could be calculated to be $p_{max} \approx 0.31$ *via* the formula $p_{PS\text{-}BBA} = V/[a \times (l_{PS} + l_B)]$. Therefore, the macromolecule would only adopt a cone-shaped conformation and form spheres with any initial concentration of PS-BBA. At the same time, the cone-angle may decrease due to the smaller heads; thus more molecules will assemble into one sphere as the concentration increases. This is evidenced from the light scattering experiments in Fig. S6 (ESI†) that the size of the spheres increases with the initial concentrations. Notably, the assumption of using the contour length of PS in the calculation is also supported by analyzing the spherical micelles of PS-BBA with an initial concentration of 0.1% as an example. By subtracting the size of APOSS and the length of the BPOSS part with linkers from the measured micelle size of about 11 nm, the calculated length of the PS part is about 4.5 nm, which is close to its fully stretched length.

While for the other sequence isomer PS-ABB, the hydrophobic PS and BPOSS are phase separated by APOSS. In order to avoid the hydrophobic moieties directly contacting with water, the molecule has to adopt a folded conformation so that both the PS and BPOSS could stay in the hydrophobic core phase. This makes PS-ABB resemble a "one head two heterogeneous tail" giant surfactant, in which one tail is PS and the other tail is two BPOSSs. The two bulky "parallel" linked tails of PS-ABB will make its assembly behavior very different from its sequence isomer PS-BBA. The maximum possible p value can be calculated to be $p_{max} \approx 0.62$ based on a similar calculation (see the ESI†). Therefore, PS-ABB has a higher tendency to form non-spherical assemblies such as cylindrical micelles or vesicles, especially at higher concentrations. When the concentration is relatively high at 1 wt%, we speculate that $p > 0.5$ and the molecule should be in the "vesicle/lamella region", in which giant surfactants usually form vesicles.[28] However, in this case, the PS-ABB molecules alternatively form nanoribbon-like assemblies containing lamellar structures within the ribbons. It is known that BPOSS is a crystalline moiety.[37–39] When the molecule is in or close to a "vesicle/lamella region", crystallization with high enthalpy may act as the driving force for forming unconventional structures.[40] In the current case, we speculate that BPOSS may have crystalized, so that a straight lamellar structure is preferred instead of vesicles. According to the literature and the above experiments, the freeze-dried self-assemblies of these giant surfactant in solution as shown in Fig. 4a could represent their true solution state.[29] So, we performed wide angle X-ray diffraction (WAXD) of the freeze-dried PS-ABB assembled nanoribbon-like structure. Fig. 3d clearly shows the diffraction peaks attributed to crystalline BPOSS,[38,41] which supports our speculation. As the concentration decreases, a_A increases and p decreases. For 0.4 wt%, the p value may decrease to below 0.5; therefore, worm-like cylindrical assemblies are observed. At the lowest concentration of 0.1%,

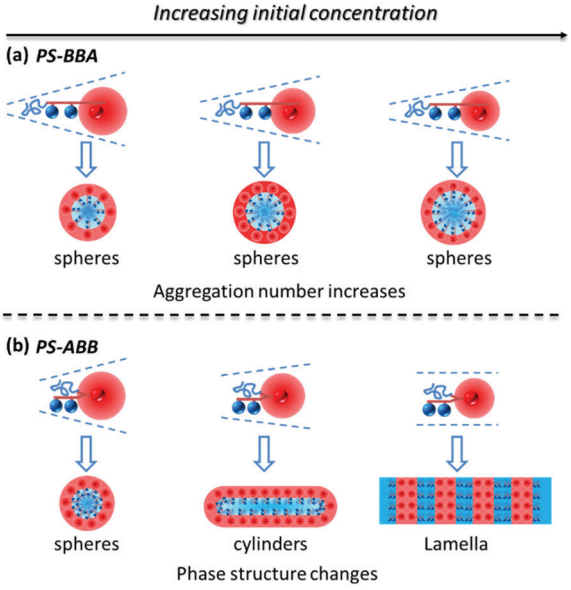

Fig. 4 Proposed models for the different assembly processes for the sequential isomers: (a) PS-BBA and (b) PS-ABB. The blue ball represents BPOSS and the red ball represents APOSS. The red corona around the red ball indicates the partially ionized APOSS, which could become smaller when the initial concentration was increased.

p may further decrease to below 0.33, the assembled structures thus become spheres. In these two cases, due to the formation of curvature structures, BPOSSs are not crystallized, which is confirmed by the WAXD spectra of the corresponding freeze-dried samples as shown in Fig. S9 (ESI†). Therefore, proposed models for the self-assembly behaviors of these two sequential isomers are shown in Fig. 4.

In addition to different self-assembly behaviors in solution, PS-ABB and PS-BBA also show differences in the bulk state. PS-ABB can also form a lamellar structure after thermal annealing (Fig. S10a, ESI†), but only a disordered structure can be observed in the PS-BBA sample (Fig. S10b, ESI†).

To conclude, we have designed and synthesized two giant surfactants with exactly the same composition but different sequences, PS-ABB and PS-BBA. The distinct nanoparticle sequences in the giant molecules could lead to different macromolecular conformations, which could further affect their self-assembly behaviors in DMF/water solution. The conjugate of PS-BBA, which resembles a ''one head one tail'' giant surfactant, can only form spherical assemblies. On the other hand, the conjugate of PS-ABB, which resembles a ''one head two heterogeneous tail'' giant surfactant, can form spheres, cylinders or a nanoribbon-like structure in response to different initial concentrations. With the growing field of sequence-controlled oligomer/polymer chemistry, these results further support the importance of sequence-control in synthetic macromolecules, which can have dramatic impacts on their self-assembled structures and macromolecular properties.

This work was supported by NSF (DMR-1408872, CHE-1808115) and NSFC (51603133). This research used resources of the Advanced Photon Source, a U.S. Department of Energy (DOE) Office of Science User Facility operated for the DOE Office of Science by Argonne National Laboratory under Contract No. DE-AC02-06CH11357.

Conflicts of interest

There are no conflicts to declare.

Notes and references

1 M. L. McKee, P. J. Milnes, J. Bath, E. Stulz, A. J. Turberfield and R. K. O'Reilly, *Angew. Chem., Int. Ed.*, 2010, **49**, 7948–7951.
2 M. Porel and C. A. Alabi, *J. Am. Chem. Soc.*, 2014, **136**, 13162–13165.
3 Y.-H. Wu, J. Zhang, F.-S. Du and Z.-C. Li, *ACS Macro Lett.*, 2017, **6**, 1398–1403.
4 A. Anastasaki, B. Oschmann, J. Willenbacher, A. Melker, M. H. C. Van Son, N. P. Truong, M. W. Schulze, E. H. Discekici, A. J. McGrath, T. P. Davis, C. M. Bates and C. J. Hawker, *Angew. Chem., Int. Ed.*, 2017, **56**, 14483–14487.
5 S. Martens, J. Van den Begin, A. Madder, F. E. Du Prez and P. Espeel, *J. Am. Chem. Soc.*, 2016, **138**, 14182–14185.
6 Y. Hibi, M. Ouchi and M. Sawamoto, *Nat. Commun.*, 2016, **7**, 11064.
7 W. Xi, S. Pattanayak, C. Wang, B. Fairbanks, T. Gong, J. Wagner, C. J. Kloxin and C. N. Bowman, *Angew. Chem., Int. Ed.*, 2015, **54**, 14462–14467.
8 W. Zhang, M. Huang, H. Su, S. Zhang, K. Yue, X.-H. Dong, X. Li, H. Liu, S. Zhang, C. Wesdemiotis, B. Lotz, W.-B. Zhang, Y. Li and S. Z. D. Cheng, *ACS Cent. Sci.*, 2016, **2**, 48–54.
9 D. Debnath, J. A. Baughman, S. Datta, R. A. Weiss and C. Pugh, *Macromolecules*, 2018, **51**, 7951–7963.
10 S. C. Solleder and M. A. R. Meier, *Angew. Chem., Int. Ed.*, 2014, **53**, 711–714.
11 A. Al Ouahabi, L. Charles and J.-F. Lutz, *J. Am. Chem. Soc.*, 2015, **137**, 5629–5635.
12 A. A. Ouahabi, M. Kotera, L. Charles and J.-F. Lutz, *ACS Macro Lett.*, 2015, 1077–1080.
13 Y. Ji, L. Zhang, X. Gu, W. Zhang, N. Zhou, Z. Zhang and X. Zhu, *Angew. Chem., Int. Ed.*, 2017, **56**, 2328–2333.
14 J.-F. Lutz, M. Ouchi, D. R. Liu and M. Sawamoto, *Science*, 2013, **341**, 1238149.
15 J. Sun, A. A. Teran, X. Liao, N. P. Balsara and R. N. Zuckermann, *J. Am. Chem. Soc.*, 2013, **135**, 14119–14124.
16 C. Leng, H. G. Buss, R. A. Segalman and Z. Chen, *Langmuir*, 2015, **31**, 9306–9311.
17 Y. Suzuki, G. Cardone, D. Restrepo, P. D. Zavattieri, T. S. Baker and F. A. Tezcan, *Nature*, 2016, **533**, 369–373.
18 R. V. Thaner, Y. Kim, T. I. N. G. Li, R. J. Macfarlane, S. T. Nguyen, M. Olvera de la Cruz and C. A. Mirkin, *Nano Lett.*, 2015, **15**, 5545–5551.
19 C. Laure, D. Karamessini, O. Milenkovic, L. Charles and J.-F. Lutz, *Angew. Chem., Int. Ed.*, 2016, **55**, 10722–10725.
20 J.-F. Lutz, J.-M. Lehn, E. W. Meijer and K. Matyjaszewski, *Nat. Rev. Mater.*, 2016, **1**, 16024.
21 M. Porel, D. N. Thornlow, N. N. Phan and C. A. Alabi, *Nat. Chem.*, 2016, **8**, 590–596.
22 J. Li, R. M. Stayshich and T. Y. Meyer, *J. Am. Chem. Soc.*, 2011, **133**, 6910–6913.
23 M. R. Golder, Y. Jiang, P. E. Teichen, H. V. T. Nguyen, W. Wang, N. Milos, S. A. Freedman, A. P. Willard and J. A. Johnson, *J. Am. Chem. Soc.*, 2018, **140**, 1596–1599.
24 W. Zhang, X. Lu, J. Mao, C.-H. Hsu, G. Mu, M. Huang, Q. Guo, H. Liu, C. Wesdemiotis, T. Li, W.-B. Zhang, Y. Li and S. Z. D. Cheng, *Angew. Chem., Int. Ed.*, 2017, **56**, 15014–15019.
25 W.-B. Zhang, X. Yu, C.-L. Wang, H.-J. Sun, I. F. Hsieh, Y. Li, X.-H. Dong, K. Yue, R. Van Horn and S. Z. D. Cheng, *Macromolecules*, 2014, **47**, 1221–1239.
26 K. Yue, M. Huang, R. L. Marson, J. He, J. Huang, Z. Zhou, J. Wang, C. Liu, X. Yan, K. Wu, Z. Guo, H. Liu, W. Zhang, P. Ni, C. Wesdemiotis, W.-B. Zhang, S. C. Glotzer and S. Z. D. Cheng, *Proc. Natl. Acad. Sci. U. S. A.*, 2016, **113**, 14195–14200.
27 W. Zhang, S. Zhang, Q. Guo, X. Lu, Y. Liu, J. Mao, C. Wesdemiotis, T. Li, Y. Li and S. Z. D. Cheng, *ACS Macro Lett.*, 2018, **7**, 635–640.
28 X. Yu, Y. Li, X.-H. Dong, K. Yue, Z. Lin, X. Feng, M. Huang, W.-B. Zhang and S. Z. D. Cheng, *J. Polym. Sci., Part B: Polym. Phys.*, 2014, **52**, 1309–1325.
29 X. Yu, S. Zhong, X. Li, Y. Tu, S. Yang, R. M. Van Horn, C. Ni, D. J. Pochan, R. P. Quirk, C. Wesdemiotis, W.-B. Zhang and S. Z. D. Cheng, *J. Am. Chem. Soc.*, 2010, **132**, 16741–16744.
30 X. Yu, W.-B. Zhang, K. Yue, X. Li, H. Liu, Y. Xin, C.-L. Wang, C. Wesdemiotis and S. Z. D. Cheng, *J. Am. Chem. Soc.*, 2012, **134**, 7780–7787.
31 Y. Chu, W. Zhang, X. Lu, G. Mu, B. Zhang, Y. Li, S. Z. D. Cheng and T. Liu, *Chem. Commun.*, 2016, **52**, 8687–8690.
32 W. Zhang, Y. Chu, G. Mu, S. A. Eghtesadi, Y. Liu, Z. Zhou, X. Lu, M. A. Kashfipour, R. S. Lillard, K. Yue, T. Liu and S. Z. D. Cheng, *Macromolecules*, 2017, **50**, 5042–5050.
33 S. A. Eghtesadi, M. A. Kashfipour, X. Sun, W. Zhang, R. S. Lillard, S. Z. D. Cheng and T. Liu, *Nanoscale*, 2018, **10**, 1411–1419.
34 Y. Li, X.-H. Dong, Y. Zou, Z. Wang, K. Yue, M. Huang, H. Liu, X. Feng, Z. Lin, W. Zhang, W.-B. Zhang and S. Z. D. Cheng, *Polymer*, 2017, **125**, 303–329.
35 R. Nagarajan, *Langmuir*, 2002, **18**, 31–38.
36 K. Wu, M. Huang, K. Yue, C. Liu, Z. Lin, H. Liu, W. Zhang, C.-H. Hsu, A.-C. Shi, W.-B. Zhang and S. Z. D. Cheng, *Macromolecules*, 2014, **47**, 4622–4633.
37 L. Cui, J. P. Collet, G. Xu and L. Zhu, *Chem. Mater.*, 2006, **18**, 3503–3512.
38 M. Huang, C.-H. Hsu, J. Wang, S. Mei, X. Dong, Y. Li, M. Li, H. Liu, W. Zhang, T. Aida, W.-B. Zhang, K. Yue and S. Z. D. Cheng, *Science*, 2015, **348**, 424–428.
39 H. Liu, J. Luo, W. Shan, D. Guo, J. Wang, C.-H. Hsu, M. Huang, W. Zhang, B. Lotz, W.-B. Zhang, T. Liu, K. Yue and S. Z. D. Cheng, *ACS Nano*, 2016, **10**, 6585–6596.
40 J. Zhang, L.-Q. Wang, H. Wang and K. Tu, *Biomacromolecules*, 2006, **7**, 2492–2500.
41 A. J. Waddon and E. B. Coughlin, *Chem. Mater.*, 2003, **15**, 4555–4561.

Supporting Information

Sequence Isomeric Giant Surfactants with Distinct Self-Assembly Behaviors in Solution

Wei Zhang,[a] Wenpeng Shan,[a] Shuailin Zhang,[a] Yuchu Liu,[a] Hao Su,[b] Jiancheng Luo,[a] Yanfeng Xia,[a] Tao Li,[c,d] Chrys Wesdemiotis,[a,e] Tianbo Liu,[a] Honggang Cui,[b] Yiwen Li,[f]* Stephen Z.D. Cheng[a,g]*

[a] Department of Polymer Science, College of Polymer Science and Polymer Engineering, The University of Akron, Akron, Ohio, 44325-3909, USA

[b] Department of Chemical and Biomolecular Engineering, The Johns Hopkins University, Baltimore, MD 21218, USA

[c] X-ray Science Division, Advanced Photon Source, Argonne National Laboratory, Argonne, Illinois, 60439, USA

[d] Department of Chemistry and Biochemistry Northern Illinois University, DeKalb, IL 60115, USA

[e] Department of Chemistry, The University of Akron, Akron, Ohio 44325-3601, USA

[f] College of Polymer Science and Engineering, State Key Laboratory of Polymer Materials Engineering, Sichuan University, Chengdu, 610065, China

[g] South China Advanced Institute for Soft Matter Science and Technology, South China University of Technology, Guangzhou, China, 510640

*S.Z.D.C., e-mail scheng@uakron.edu;

*Y.L., e-mail ywli@scu.edu.cn.

Methods and Characterizations

^{1}H NMR experiments were measured on a Varian Mercury 500 NMR spectrometer. The spectra were referenced to the residual solvent peak in $CDCl_3$ at δ 7.27 ppm.

Gel permeation chromatography (GPC) were measured in THF at 35 °C on Tosoh EcoSEC instrument with three columns [TSKgel SuperH3000 x 2, TSKgel SuperH5000] with a Guard Column (TSKgel SuperH1000-4000) and a UV detector.

Matrix-assisted laser desorption/ionization time-of-flight (MALDI-TOF) mass spectra were measured on a Bruker Ultra flex III TOF/TOF mass spectrometer equipped with a Nd:YAG laser emitting at 355 nm. Trans-2-[3-(4-tert-butylphenyl)-2-methyl-2-propenyli-dene]-malononitrile (DCTB, >98%, Sigma-Aldrich) was dissolved in THF (20.0 mg/mL) as the matrix solution. Sodium trifluoroacetate (NaTFA, 98%, Sigma-Aldrich), potassium trifluoroacetate (KTFA, 98%, Sigma-Aldrich), or silver trifluoroacetate (AgTFA, 98%, Sigma-Aldrich) was dissolved in MeOH/$CHCl_3$ (v/v = 1/3) at 10.0 mg/mL and used as the cationizing agent solution. The matrix and cationizing agent solutions were mixed in a 10/1 (v/v) ratio. Samples were typically dissolved in THF at 5.0 mg/mL. To prepare the samples, 0.5 μL of the matrix and cationizing agent mixture solution was deposited on the wells of a 384-well ground-steel sample plate and allowed to dry, followed by depositing 0.5 μL of the sample solution on a spot of the dried matrix and cationizing agent, and a second deposition of 0.5 μL of the matrix and cationizing agent mixture solution on top of the dried sample. The sample plate was loaded into the MALDI-TOF mass spectrometer and the spectra were measured in the reflection mode. Data analyses were conducted using the Bruker's flexAnalysis software.

A typical preparation process for the solution assembled samples was to first completely dissolve the material in DMF with a certain initial concentration. Then, water was added dropwise at a rate of 20 μL/hour until the water content reached 50%. The solution was then dialyzed in water using a dialysis tube with molecular weight cutoff of 20k.

For the bulk state self-assembly studies, a piece of sample was thermal annealed for 1h at different temperatures (70-120 ^{o}C) to find the best condition and measured in small angle X-ray scattering (SAXS) experiments.

Dynamic light scattering (DLS) experiments were conducted on a commercial Brookhaven laser scattering spectrometer equipped with a 532 nm laser. An intensity-intensity BI-9000AT correlator was used to get the correlation function based on the particle movement. The diffusion coefficient D could be obtained by $\Gamma=Dq^2$, which Γ was calculated by CONTIN method. The hydrodynamic radius (R_h) can be calculated according to the Stokes-Einstein equation: $R_h=k_bT/6\pi\eta D$ in which k_b is the Boltzmann constant and η is the viscosity of the solution.

A JEOL JEM-2000 electron microscope operated at 200 kV was used for obtaining the images. The samples were prepared by dropping the solution on a copper grid coated with a thin carbon film. After about 30s, the excess solution was removed by a piece of filter paper, and the sample was dried at room temperature for overnight.

Cryo-TEM imaging was performed for the dialyzed solution of the nano-belt like structure. 6 μL of the sample solution was added onto a lacey carbon film supported TEM copper grid (Electron Microscopy Services, Hatfield, PA, USA), which was pre-treated

with plasma air. A thin ice layer of sample was produced using the Vitrobot (FEI). After dropping of the sample solution, the lacey carbon grid was blotted and plunged instantly into a liquid ethane reservoir precooled by liquid nitrogen. The vitrified samples were then transferred to a cryo-holder and cryo-transfer stage that was cooled by liquid nitrogen. During the imaging process, temperature of the cryo-holder was maintained below -170°C with liquid nitrogen to prevent sublimation of vitreous water. All images were recorded by a 16 bit 2K × 2K FEI Eagle bottom mount camera.

The samples were freeze dried before the wide angle X-ray diffraction (WAXD) experiments, which were performed on an instrument with a Rigaku 18 kW rotating anode generator and an image plate detector. The instrument was calibrated using silicon powders with 2θ of 28.4° under Cu Kα radiation. The air scattering was subtracted. The 1D WAXD curve was analyzed and integrated from the 2D image using a Rigaku software.

Synchrotron SAXS experiments were conducted at 12-ID-B, C station with X-ray energy of 12 keV at the Advanced Photon Source (APS) of Argonne National Laboratory. The sample-to-detector distance was adjusted to provide a detecting range for scattering vector $q = 4\pi(\sin\theta)/\lambda$ between 0.001 to 0.60 $Å^{-1}$, calibrated using a silver behenate standard. A CCD area detector was used, and the typical exposure time was 0.1 s for each sample.

Chemicals and Materials

All the chemicals and solvents were used as received from Sigma-Aldrich, Acros Organic, or Fisher Scientific. PS-N_3, DIBO-V-CHO, DIBO-B-CHO, the “click adaptor”, DIBO-V and DIBO-B were prepared as we previously reported.[1-3]

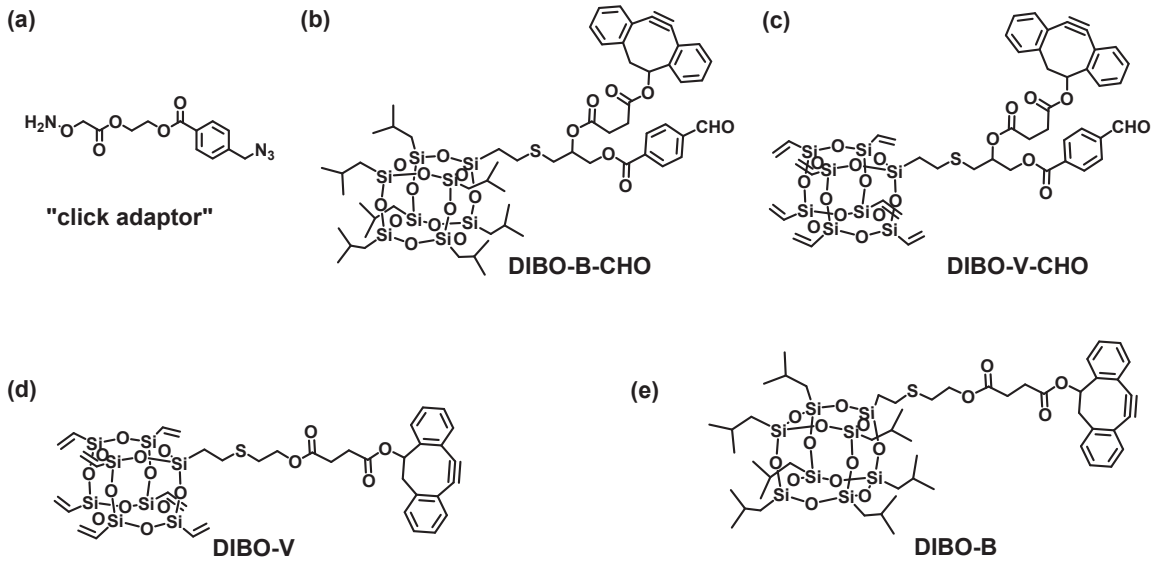

Scheme S1. Chemical structures of building blocks: (a) the "click adaptor;[3] (b) DIBO-B-CHO;[1] (c) DIBO-V-CHO;[1] (d) DIBO-V;[2] (e) DIBO-B.[2]

A typical procedure of SPAAC reactions: The corresponding azido terminated giant molecule (1.0 eq.) and DIBO-V-CHO or DIBO-B-CHO or DIBO-V or DIBO-B (1.05 eq. per -N3) were fully dissolved in THF (3 mL). The mixture was stirred at ambient environment for 5 hours. Then, the solution was concentrated, followed by precipitation into cold methanol three times.

A typical procedure of oxime ligations: The corresponding aldehyde terminated giant molecules (1.0 eq.) was dissolved in THF (3mL), followed by the addition of the "click adaptor" (1.2 eq. per -CHO). The mixture was stirred for about 2 h to complete the reaction, as monitored by crude ^{1}H NMR. Purification was performed by repeated precipitation in cold methanol.

A typical procedure of TECCs. The corresponding precursors containing VPOSS, 2 e.q. of thioglycolic acid to 1 e.q. vinyl group and 0.03 eq of photoinitiator 2-hydroxy-4'-(2-hydroxyethoxy)-2-methylpropiophenone (Irgacure 2959) were fully dissolved in THF (3mL). The solution was illuminated under 365 nm light in the UV reactor for 10 min. Then the solution was concentrated and precipitated into methanol/water 1:5. The products were collected by filtration.

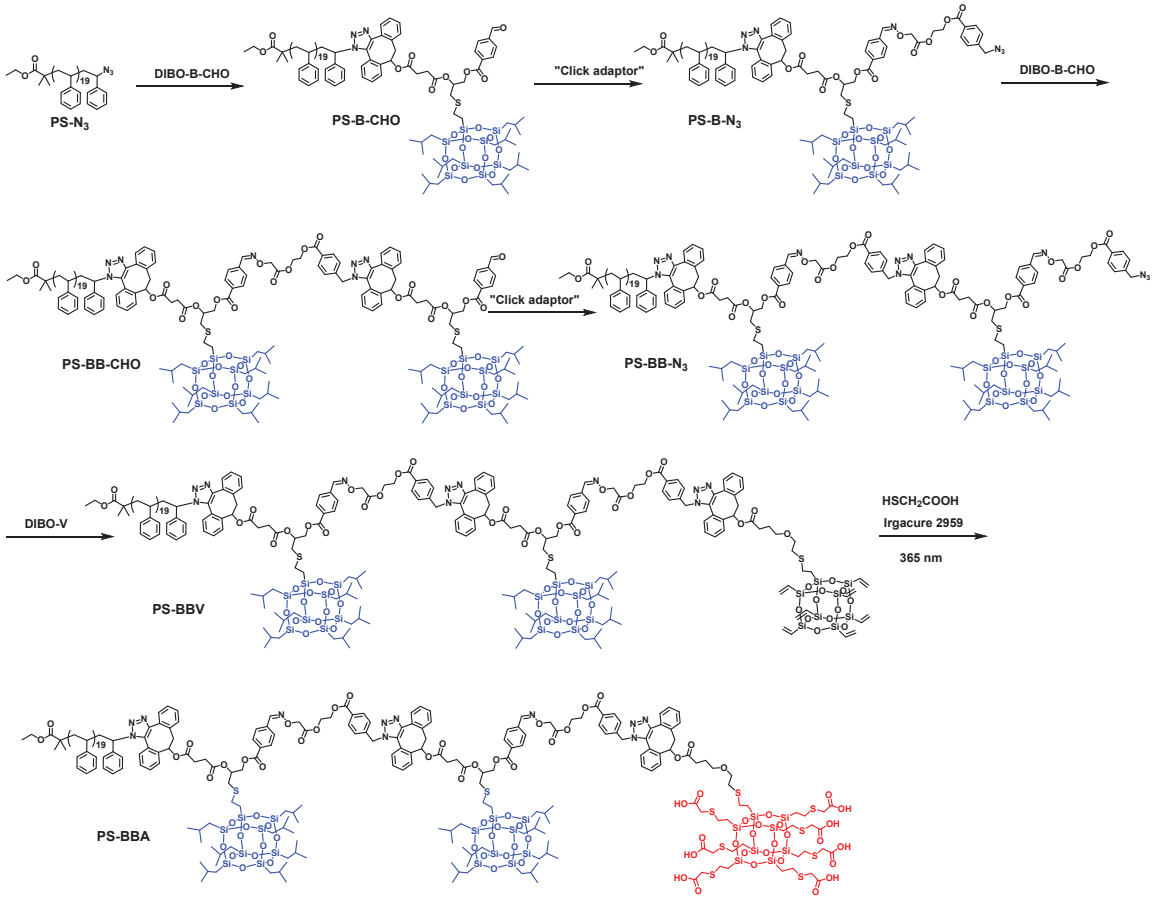

Scheme S2. Synthetic route towards PS-BBA.

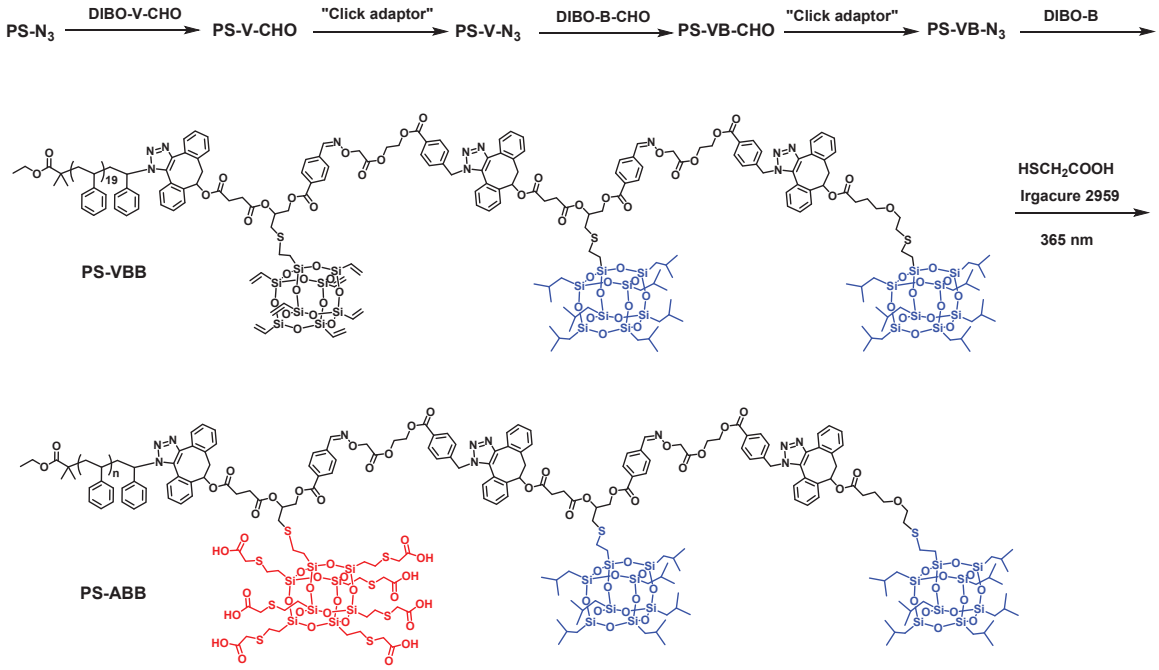

Scheme S3. Synthetic route towards PS-ABB.

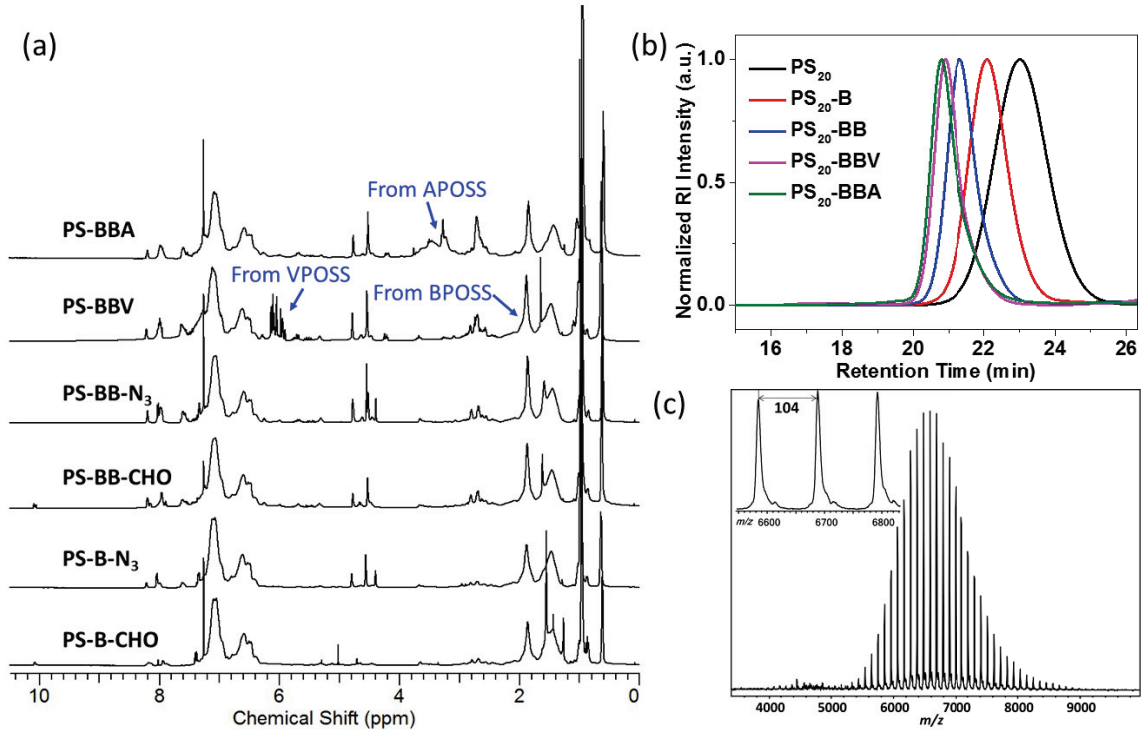

Figure S1. (a) 1H NMR spectra and (b) GPC of PS-BBA and related intermediates; (c) MALDI-TOF spectrum of PS-BBV (The inset figure is zoomed in. The distance between each peak is 104, which corresponds to the molecular weight of one styrene unit.).

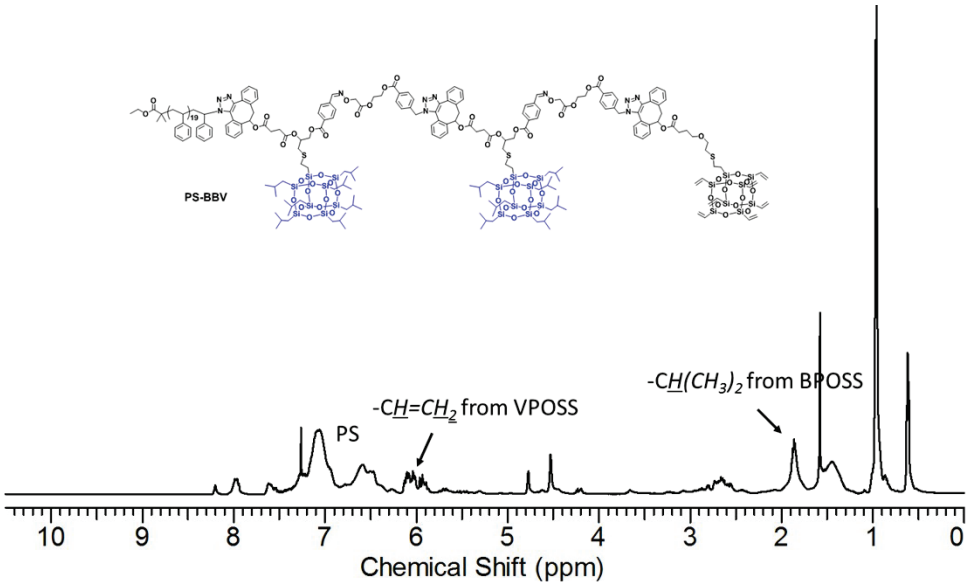

Figure S2. ^{1}H NMR spectrum of PS-VBB.

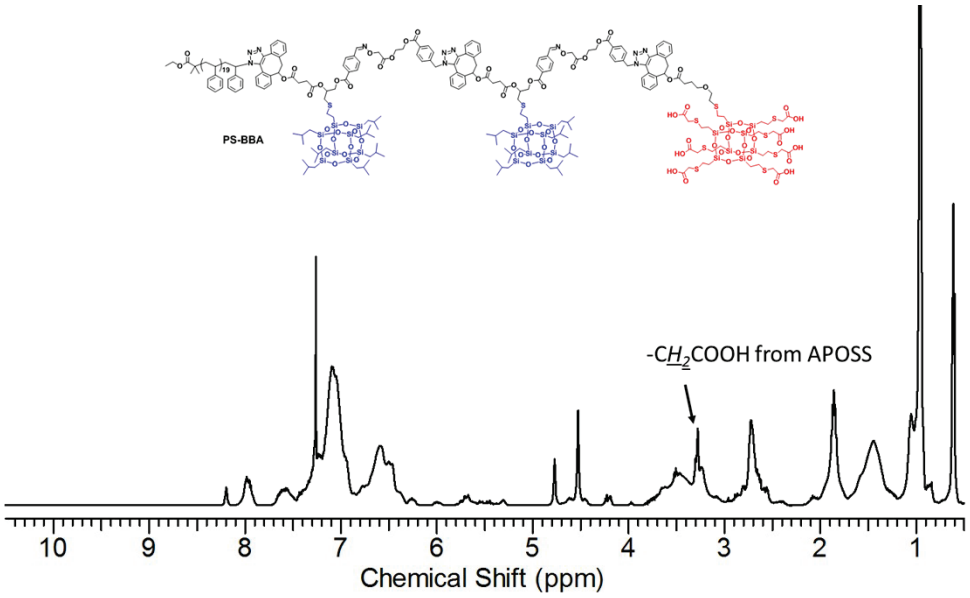

Figure S3. ^{1}H NMR spectrum of PS-ABB.

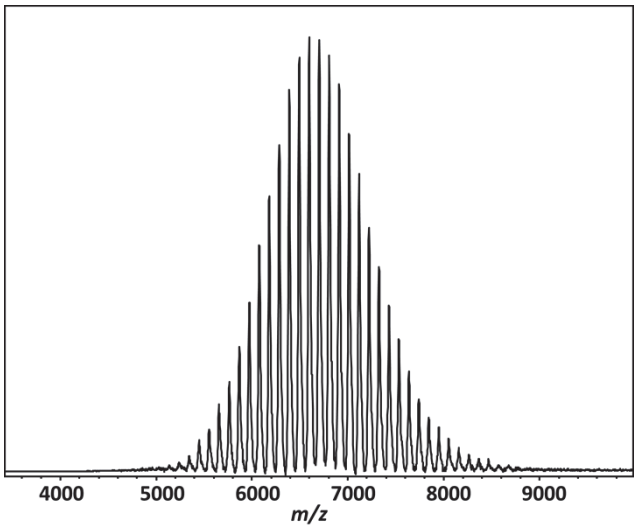

Figure S4. MALDI-TOF spectrum of PS-VBB

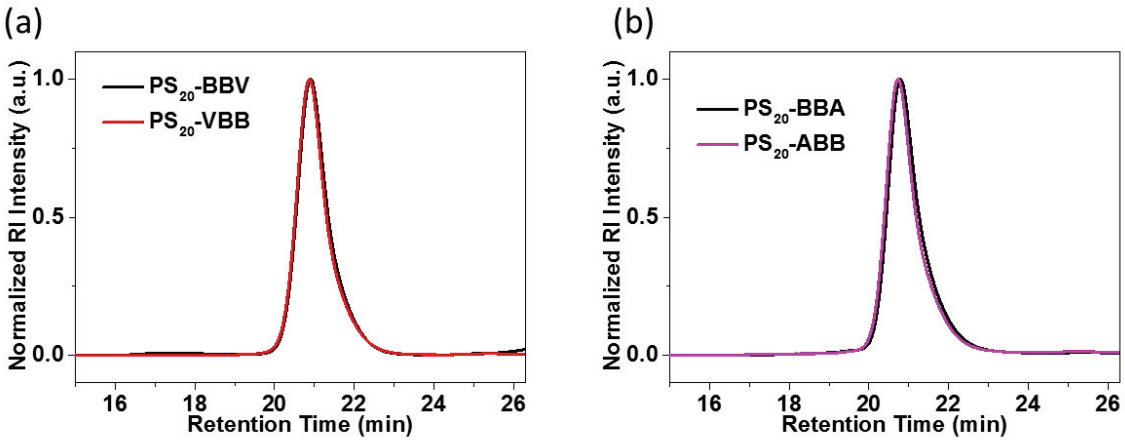

Figure S5. GPC curves of (a) PS-BBV and PS-VBB (b) PS-BBA and PS-ABB. Due to the same composition, the curve of PS-BBV almost overlap with that of PS-VBB, and the curve of PS-BBA almost overlap with that of PS-ABB.

Estimation of the Packing Parameters

For both PS-BBA and PS-ABB, due to their same composition, the volume of the hydrophobic part (V) is identical and can be estimated by the following calculation:

$$V = V_B + V_{PS} = \frac{M_B}{N_A \rho_B} + \frac{M_{Ps}}{N_A \rho_{PS}}$$

$$= \frac{1.6 kg/mol}{6.02 mol^{-1} \times 1.1\ g/cm^3} + \frac{2 kg/mol}{6.02 mol^{-1} \times 1.04\ g/cm^3} = 5.6\ nm^3$$

where V_B and V_{PS} are the volume of the BPOSS and PS parts, respectively; M_B = 1.6 kg/mol (for simplification we include the linker as well) and M_{PS} = 2 kg/mol are the molecular masses of the BPOSS and PS parts, respectively; ρ_B = 1.1 g/cm^3 and ρ_{PS} = 1.04 g/cm^3 are their densities;[4] and N_A is the Avogadro constant.

The contour length of polystyrene tail (l_{PS}) can be estimated about 5 nm by l = 0.154$n$sin(109.5^o/2), where n = 40 (two carbons per repeat unit). The length of BPOSS part with the linkers (l_B) is also about 5 nm.When assuming no ionization of APOSS, according to its diameter of about 1.5nm, the smallest cross section area of APOSS (a_A) can be estimated as:

$$a_A = (d/2)^2\pi = 1.8\ nm^2$$

Since PS and BPOSS are "serially" linked in PS-BBA, by assuming no ionization of APOSS when the cross-section area of APOSS is the smallest, the maximum possible value of the packing parameter p for PS-BBA can be estimated as:

$$p_{\text{PS-BBA(max)}} = V/[a\times(l_{\text{PS}} + l_{\text{B}})] = 5.6\ \text{nm}^3/[1.8\ \text{nm}^2\times(5\ \text{nm} + 5\ \text{nm})] = 0.31$$

Since PS and BPOSS are "parallelly" linked in PS-ABB, by assuming no ionization of APOSS when the cross-section area of APOSS is the smallest, similarly, the maximum possible value of the packing parameter p for PS-ABB can be estimated as:

$$p_{\text{PS-ABB(max)}} = V/(a\times l) = 5.6\ \text{nm}^3/(1.8\ \text{nm}^2\times 5\ \text{nm}) = 0.62$$

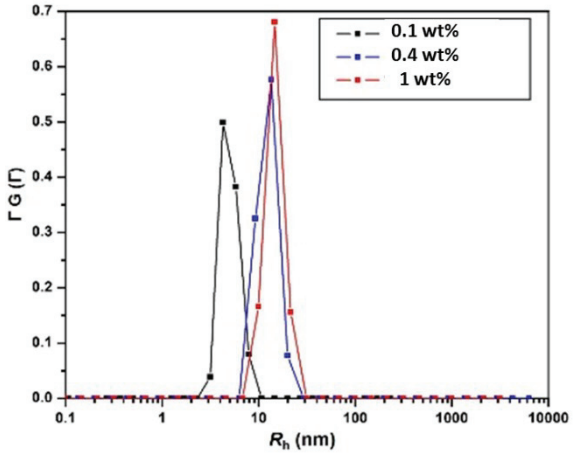

Figure S6. CONTIN analysis of DLS data of PS-BBA in DMF/water with different initial concentrations (0.1 wt%, 0.4 wt% and 1 wt%).

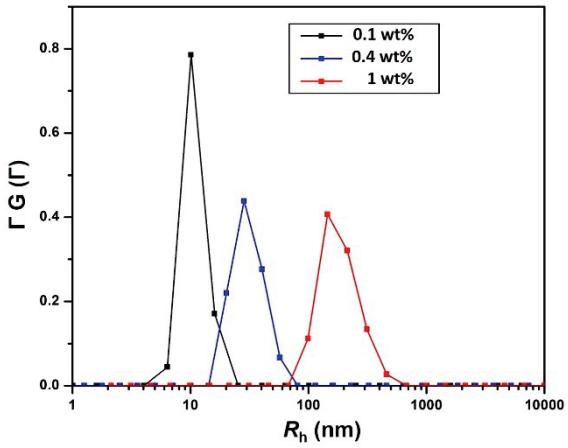

Figure S7. CONTIN analysis of DLS data of PS-ABB in DMF/water with different initial concentrations (0.1 wt%, 0.4 wt% and 1 wt%).

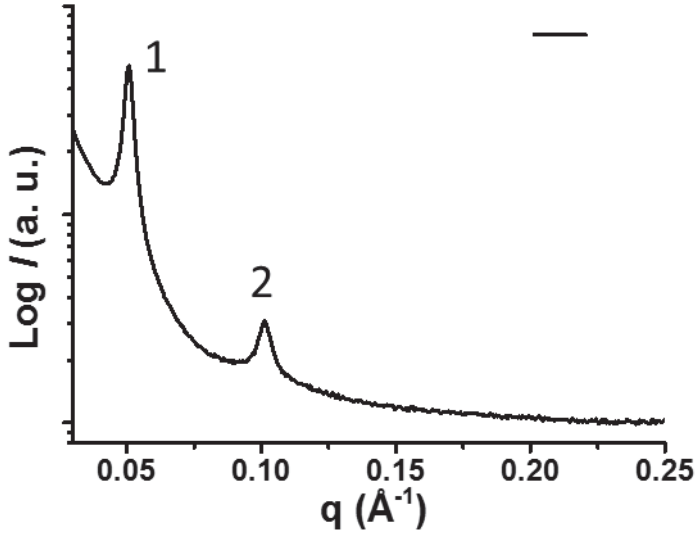

Figure S8. SAXS profile of the freeze-dried "nano-belt" structure of PS-ABB.

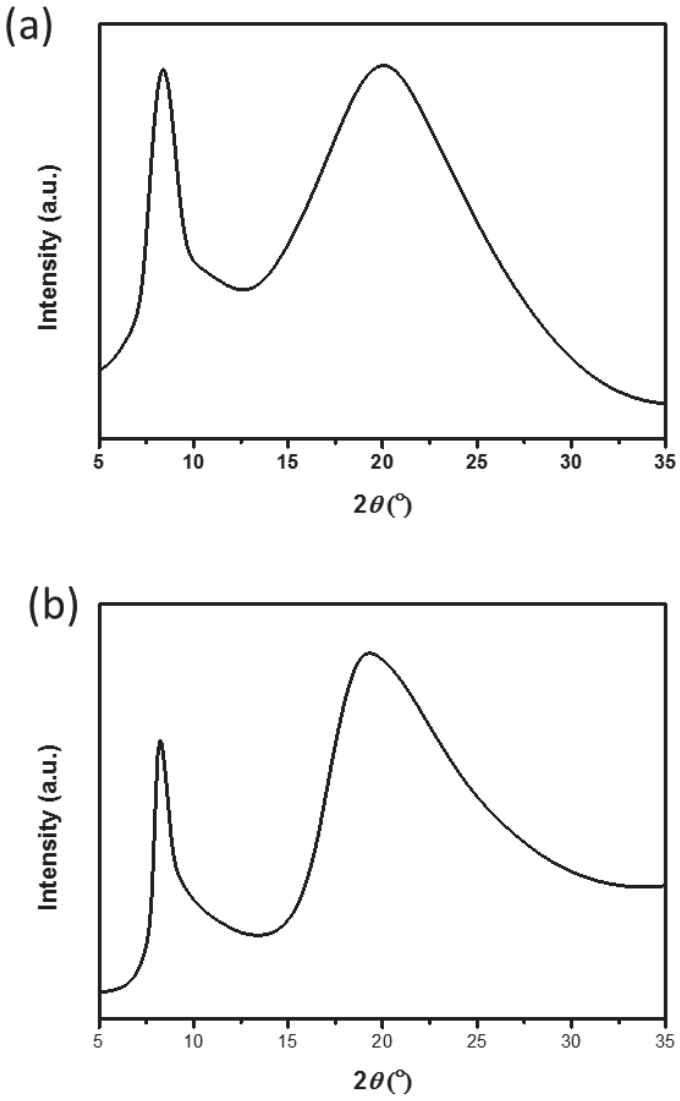

Figure S9. WAXD spectra of PS-ABB from the freeze-dried assembled solution with initial concentration of (a) 0.1 wt% and (b) 0.4 wt%. Those data show no crystallization of BPOSS.

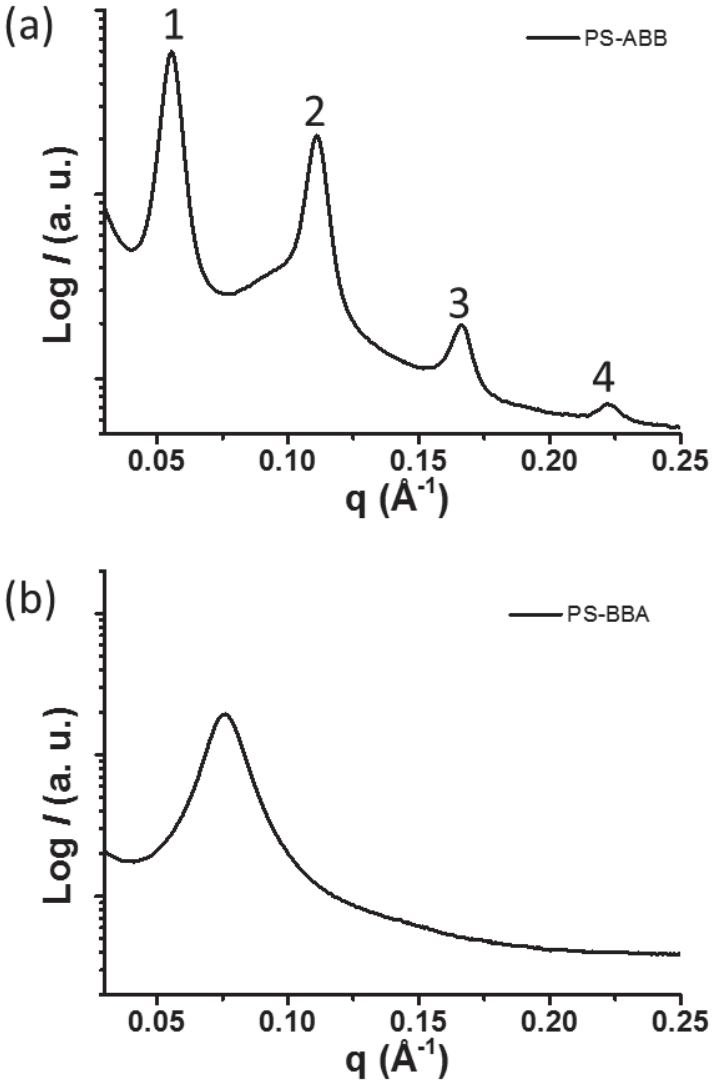

Figure S10. (a) SAXS profile of PS-ABB in the bulk state after annealing at 100 ^{o}C, which shows *q* ratio of 1:2:3:4, indicating a lamellar structure. (b) SAXS profile of PS-BBA in the bulk state after thermal annealing at 100 ^{o}C, which shows no ordered structure. The results indicate that the two "sequence isomers" also show different assembly behavior in the bulk state.

References:

1. W. Zhang, M. Huang, H. Su, S. Zhang, K. Yue, X.-H. Dong, X. Li, H. Liu, S. Zhang, C. Wesdemiotis, B. Lotz, W.-B. Zhang, Y. Li and S. Z. D. Cheng, *ACS Cent. Sci.*, 2016, **2**, 48-54.
2. W. Zhang, S. Zhang, Q. Guo, X. Lu, Y. Liu, J. Mao, C. Wesdemiotis, T. Li, Y. Li and S. Z. D. Cheng, *ACS Macro Lett.*, 2018, **7**, 635-640.
3. H. Su, Y. Li, K. Yue, Z. Wang, P. Lu, X. Feng, X.-H. Dong, S. Zhang, S. Z. D. Cheng and W.-B. Zhang, *Polym. Chem.*, 2014, **5**, 3697-3706.
4. K. Wu, M. Huang, K. Yue, C. Liu, Z. Lin, H. Liu, W. Zhang, C.-H. Hsu, A.-C. Shi, W.-B. Zhang and S. Z. D. Cheng, *Macromolecules*, 2014, **47**, 4622-4633.